Chinese Journal of Chemical Engineering 76 (2024) 201–210

Contents lists available at ScienceDirect

Chinese Journal of Chemical Engineering

journal homepage: www.elsevier.com/locate/CJChE

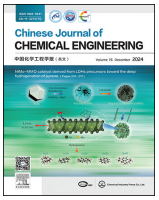

Full Length Article

NiMo-MMO catalyst derived from LDHs precursors toward the deep hydrogenation of pyrene

Yongliang Jia [1, 2, 3, 4, 5], Boyang Bai [1, 6], Jing Wang [1, 2, 3, 4, 5], Yueyi Wang [1, 2, 3, 4, 5], Zheng Wang [1, 2, 3, 4, 5], Xiaoxun Ma [1, 2, 3, 4, 5, *]

[1] *School of Chemical Engineering, Northwest University, Xi'an 710069, China*
[2] *International Scientific and Technological Cooperation Base of the Ministry of Science and Technology (MOST) for Clean Utilization of Hydrocarbon Resources, Xi'an 710069, China*
[3] *Chemical Engineering Research Center of the Ministry of Education (MOE) for Advanced Use Technology of Shanbei Energy, Xi'an 710069, China*
[4] *Shaanxi Research Center of Engineering Technology for Clean Coal Conversion, Xi'an 710069, China*
[5] *Collaborative Innovation Center for Development of Energy and Chemical Industry in Northern Shaanxi, Xi'an 710069, China*
[6] *College of Chemistry and Materials Science, Weinan Normal University, Weinan 714000, China*

A R T I C L E I N F O

Article history:
Received 13 March 2024
Received in revised form
20 September 2024
Accepted 22 September 2024
Available online 11 October 2024

Keywords:
$Ni@Al_2O_3$LDHs
Structural topological transformation method
NiMo-MMO catalyst
Pyrene deep hydrogenation

A B S T R A C T

A series of Ni-based catalysts were prepared *via* structural topological transformation from the $Ni@Al_2O_3$ layered double hydroxides (LDHs) precursors, and applied for the deep catalytic hydrogenation saturation of pyrene in a high-pressure reactor. The pore structures, active species dispersion, surface morphology, amount and type of acid of the prepared catalysts were characterized by BET, XRD, SEM, TEM, XPS, SEM, NH_3-TPD and Py-IR. We studied the influence of physicochemical properties of Ni-based catalysts on the regularity and mechanism of deep hydrogenation of pyrene. Meanwhile, the synergy between Ni and Mo, and the interaction between active metals and support were discussed to further reveal the constitutive relationship during the hydrogenation reaction of pyrene. The results of the evaluation of the catalytic hydrogenation of pyrene show that the as-prepared NiMo mixed metal oxide (MMO) catalyst showed excellent catalytic activity: ~95% pyrene conversion, 90.12% for the selectivity of deep hydrogenation products (hexahydropyrene, decahydropyrene and hexadecahydropyrene). It was expected that the successfully preparation and utilization of NiMo-MMO catalyst could provide a theoretical basis for the design of this kind of catalysts for deep catalytic hydrogenation of polycyclic aromatic hydrocarbons (PAHs).

1. Introduction

Coal is an important energy resources in the world, particularly in China, where the coal production and consumption over 50% of the world's total [1]. As a by-product of the coal carbonization, high-temperature coal tar (HTCT) has a high annual output. In recent years, China's annual off-take potential of HTCT has reached approximately 26 Mt, which consists of 95% PAHs [2]. PAHs is the important raw material for preparing medicines, hydrogen donors, dyes, and pesticides [3]. Therefore, the processing and utilization of PAHs has received increasing attention in the past few years, particularly, the hydrogenation of PAHs [4]. The deep hydrogenation of PAHs is a clean and efficient process that is important for the value-added application of HTCT [5]. In reactions of hydrogenation and dehydrogenation, low molecular weight PAHs (mainly naphthalene, anthracene and phenanthrene) have been extensively investigated [6,7]. However, the intrinsic properties of highly condensed PAHs make their hydrogenation susceptible to thermodynamic and kinetic constraints, as well as strong effects of resonance, steric hindrance, and competitive adsorption [8]. Thus, choosing suitable high molecular weight dense ring aromatic hydrocarbons as a model compound allows for a better understanding of the hydrogenation mechanism of PAHs. PY is a complex tetracyclic aromatic hydrocarbon, and the hydrogenation products of PY are high value-added materials in the petroleum and pharmaceutical industry [9], which could be regarded as a model for studying the hydrogenation of PAHs.

* Corresponding author. School of Chemical Engineering, Northwest University, Xi'an 710069, China.
E-mail address: maxym@nwu.edu.cn (X. Ma).

https://doi.org/10.1016/j.cjche.2024.09.010

It is proved that precious metals exhibited excellent catalytic performance in the catalytic hydrogenation saturation of PAHs, especially Pd and Pt based catalysts are widely investigated and used [10]. However, their high cost and sensitivity to sulphur and nitrogen are not conducive to the long-term and scale-up using. Therefore, the rational design and preparation of non-noble metal catalysts with high activity and stability are crucial for the deep hydrogenation of PY [11]. The performance of non-noble metal catalysts depends not only on the types of active metal species but also on the structural properties of the materials [6]. In recent years, LDHs materials have been regarded as the good candidates for hydroprocessing reactions. This is due to their unique features, such as variable laminate and interlayer composition, stability, surface acid-base control, and atomic-level homogeneous dispersion of active metal elements [12]. LDHs materials are commonly used as precursors for layered MMO catalysts. The resulting MMO-derived catalysts have demonstrated exceptional performance in their respective catalytic reactions. Claydon *et al.* [13] prepared a Mo catalyst loaded on Ni-MMO, which exhibited performance in the deep catalytic hydrogenation of naphthalene, they found that the large, high-surface-area planar of MMO improved the homogeneous dispersion of the active species. Meng *et al.* [14] found that Ni catalysts prepared by MMO are beneficial for exposing the active sites, resulting in highly selective hydrogenation of furfural. Zhang *et al.* [15] discovered that the NiMgAl-MMO catalyst, prepared from LDHs using the hydrothermal-calcination-reduction method, exhibited a confined effect between metal oxide species. This effect efficiently promoted the dispersion of the active species. Meanwhile, in many non-homogeneous catalytic reactions, particularly hydrogenation reactions, synergistic interactions occur among the acid sites, active metal, and support on MMO-derived catalysts, which play a crucial role [16]. Additionally, mesoporous structured catalysts derived from MMO are important for the diffusion and adsorption of reactants. For instance, Claydon and Wood [17] found that a Ni-MMO catalyst with a high specific surface area and well-defined mesoporous structure exhibited a preferential capacity for adsorbing PAHs in the catalytic hydrogenation of heavy oil. It should be noted that the catalytic materials derived from MMO, as reported above, have not yet been tested with high molecular weight PAHs. Therefore, loading active metals (monometallic or bimetallic) on MMO to prepare an affordable and good activity catalyst for hydrogenation of PAHs, which is a new way of thinking to promote the deep catalytic hydrogenation saturation of PY.

In this work, three types of Ni-based catalysts were prepared on MMO support through a subsequent topological transformation and modification process. The deep hydrogenation saturation of PY was catalytically evaluated in a high-pressure reactor, and the obtained hydrogenation products were monitored/quantified by gas chromatography-mass spectrometry (GC-MS). The key influence elements of structure-performance relationship and physico-chemical properties of MMO-derived Ni-based catalysts on the deep hydrogenation characteristics of PY were investigated.

2. Experimental

2.1. Catalyst preparation

2.1.1. Synthesis of the MMO

Nanosheets with hierarchical structure of Ni, Al mixed oxides (MMO) was prepared by *in-situ* growth on the parent Al_2O_3 with urea as precipitant and hydrothermal method. Firstly, 0.02 mol of urea and 0.01 mol of Ni $(NO_3)_2\cdot 6H_2O$ were dissolved in 10 ml of distilled water, and ultrasounded for 8 min. Afterwards, 0.05 mol Al_2O_3 powder was added in the above solution with magnetic stirring for 10 min until clear. Subsequently, the obtained solution was transferred into a Teflon-lined stainless-steel autoclave and heated at 130 °C for 8 h. After cooling to room temperature, the solid product was collected, and washed with distilled water until pH = 7, and then dried at 90 °C in an oven overnight to obtain Ni@Al_2O_3 layered double hydroxides (LDHs). Finally, the catalyst precursor was calcined in a muffle at 450 °C (2 °C·min^{-1}) for 4 h. The ultimate sample was named as MMO.

2.1.2. Preparation of NiMo supported catalysts

For the 1g MMO was dispersed in distilled water (20 ml) by ultrasonication for 15 min. And then, 1.5 mmol of NH_4F, 2.47 mmol urea, 1.33 mmol of $Ni(NO_3)_2\cdot 6H_2O$, and 6.94 × 10^{-3} mmol of $(NH_4)_6Mo_7O_{24}\cdot 4H_2O$ were added to MMO, respectively. The resulting mixed aqueous solution was transferred into a hydrothermal reactor and heat-treated at 120 °C for 12 h. The solid product obtained was collected and dried at 80 °C for 5 h. Finally, the dried solid powders were calcined at 400 °C for 5 h to obtain the catalyst, which named as NiMo-MMO. The preparation process is shown in Fig. 1.

For comparison, catalyst of Ni-MMO was also prepared as the above method.

2.2. Characterization

The textural structures of the catalysts were determined using an ASAP 2460 automated gas sorption analyzer (Micromeritics, USA) through the N_2 adsorption-desorption equilibrium. The specific surface area and pore diameter were determined and calculated by Brunauer-Emmett Teller (BET) and Barrett-Joyner-Halenda (BJH) methods, respectively. The crystal texture of catalysts was identified by X-ray diffraction (XRD) using a Bruker Advance D8 XRD (40 kV, 30 mA) equipped with a Cu K_α source ($\lambda = 0.15406$ nm) and 2θ was scanned from 10° to 80° at a rate of 5 (°)·min−1. Scanning electron microscope (SEM) performed on Zeiss Sigma 300, as well as Transmission electron microscopy (TEM) and element energy dispersive spectroscopy (EDS) mapping performed on FEI Talos F200X were used to obtaining the microstructure morphology of the catalysts. The chemical characterization was performed by X-ray photoemission spectroscopy (XPS) with a Thermo Scientific K-Alpha instrument using monochromatic AlKa X-radiation (1486.6 eV). The binding energies of Ni 2p and Mo 3d were calibrated based on the graphite C 1s core level at 284.8 eV. The acidity and basicity of the catalysts were determined by temperature programmed desorption of ammonia (NH_3-TPD) using an AutochemII 2920 (Micromeritics) analyzer. Adsorbed pyridine infrared (Py-IR) analyses were performed on a Tensor 27 FTIR spectrometer (Bruker, Germany). The samples were first evacuated in situ in an IR cell. Pyridine was then adsorbed at 50 °C for 30 min and then desorbed at 150 °C for 30 min.

2.3. Catalytic hydrogenation of pyrene

Initially, pyrene(1g), cyclohexane (34 g) (effect of solvent type on pyrene hydrogenation is shown in Table S3) and catalysts (0.25 g) were joined in the autoclave and then replaced air inside the autoclave with N_2 three times. Then the temperature was raised to 340 °C and held isothermally for 2 h at this temperature with an initial hydrogen pressure of 5 MPa and a stirring rate of 60 r·min^{-1}. After the end of reaction, the supernatant from the mixture was collected when cooling the autoclave to room temperature. Furthermore, each experiment was repeated a minimum of three times under identical conditions, and the experimental samples were measured in parallel. The errors in pyrene conversion and product selectivity were within ±5%.

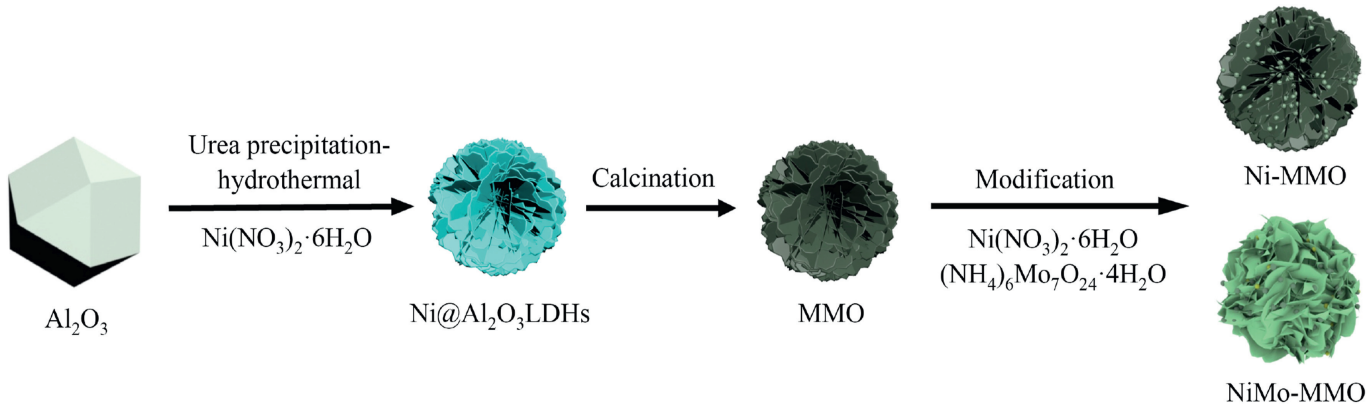

Fig. 1. The scheme of the catalyst preparation process.

The hydrogenation products of PY (structures of pyrene and the products are shown in Table S1 in the supplementary materials) were analyzed with gas chromatograph/mass spectrometer (GCMS-QP 2010 plus, Japan Shimadzu), each of compounds in products were identified in the library data *via* a probability matching method, and their relative content was determined by peak area normalization. According to the results GC-MS, various of derivatives of hydrogenation of pyrene were identified in the products were shown in Table 1 DHP will be used subsequently to represent the deep hydrogenation products (HeHP, DeHP and HHP) of PY. The conversions (Conv.) of PY and product selectivity (Sele.) were calculated based on Eqs. (1) and (2), respectively.

$$\text{Conv.} = \frac{X_{\text{in}} - X_{\text{out}}}{X_{\text{in}}} \times 100\% \quad (1)$$

$$\text{Sele.} = \frac{X_i}{X_{\text{total}}} \times 100\% \quad (2)$$

where x_{in} and x_{out} is the relative percentage content of reactant in the feedstock and product before and after the reaction, x_i and x_{total} are the relative percentage content of a certain compound in the hydrogenation product and the sum of the relative percentage content of all products, respectively.

3. Results and Discussion

3.1. Structural and property characterization of the Ni-based catalysts

3.1.1. SEM and TEM analysis

The morphology of the catalyst is crucial for its catalytic activity. Therefore, we characterized the surface morphology and crystal structure changes of the samples using SEM, as shown in Fig. 2. From Fig. 2(a), it can be seen that the original parent Al_2O_3 without any treatment displays a regular block shape with a relatively smooth and regular outer surface. However, a sample of MMO (Fig. 2(b)) composed of interconnected random stacked nanosheets was obtained after the *in-situ* growth topological transition process. This process reduced the possibility of agglomeration or aggregation of active species. Additionally, by modifying ammonium fluoride and loading active metals, as shown in Fig. 2(c), the surface of the Ni-MMO catalyst becomes denser and covered in thinner nanosheets. This is a result of the Ni species being loaded onto the catalyst. The surface of the Ni–Mo bimetallic catalyst surface in Fig. 2(d) appears to be more densely packed than the other samples. This is probably due to the interaction between Ni and Mo, which allows the active species to be well dispersed on the support. The microstructure of the NiMo-MMO composites was further investigated by TEM. As shown in Fig. 2(e), Ni–Mo bimetallic catalyst retains the structural and morphological advantages of the nanosheet material, which is beneficial for the formation of a higher degree of porous and hierarchical structure [18]. Fig. 2(f) and (g) show the TEM image of the NiMo-MMO catalyst, the lattice fringes with interplanar distances of 0.241 nm correspond to the (1 1 1) plane of NiO [19], and the average size of the Ni nanoparticles is around 8.9 nm. TEM images of Ni-MMO and NiMo-MMO catalysts are showed in Fig. S1 (in Supplementary Material), which illustrates the addition of metallic Mo did not significantly change the particle size of Ni, but effectively promoting the dispersion of active components. Meanwhile, EDS mapping (Fig. 2(h)) shows a homogeneous distribution of elements Ni, Mo, Al and O in the surface of NiMo-MMO catalyst, which is consistent with the SEM results. The high dispersion of active species distribution and the suitable particle size of the NiMo-MMO catalyst is favorable to the deep hydrogenation activity of PY.

Table 1
Compound and its abbreviation

Compound	Abbreviation
4,5-dihydropyrene	DiHP
4,5,9,10-tetrahydropyrene	TeHP
1,2,3,6,7,8-hexahydropyrene	HeHP
1,2,3,3a,4,5-hexahydropyrene (isomeric)	HeHP
1,2,3,3a,4,5,5a,6,7,8-decahydropyrene	DeHP
1,2,3,3a,7,8,9,10,10a,10b-decahydrofluoranthene (isomeric)	DeHP
Hexadecahydropyrene	HHP

3.1.2. N_2 adsorption-desorption isotherm analysis

The N_2 adsorption-desorption isotherms (Type IV) of the prepared samples are exhibited in Fig. 3(a), indicating the formation of an ordered mesoporous structure for all samples [20]. For the Al_2O_3 support, which performs isotherm with H2 shaped hysteresis loop, while H2–H3 type hysteresis loops (IUPAC classification) for the Ni-based catalysts exhibited same isotherms, indicating the presence of varying sizes and shapes pores. It might be caused by topological transformation of MMO. The pore distribution of each sample is shown in Fig. 3(b), and all samples display ordered mesoporous materials with a narrow pore distribution (3–8 nm), which was possibly attributed to uniformly sized particles active species. Details of textural structure of the Ni-based catalysts are listed in Table 2. For MMO, which possesses a lower specific surface area and pore volume compared to other samples, it may be due to the

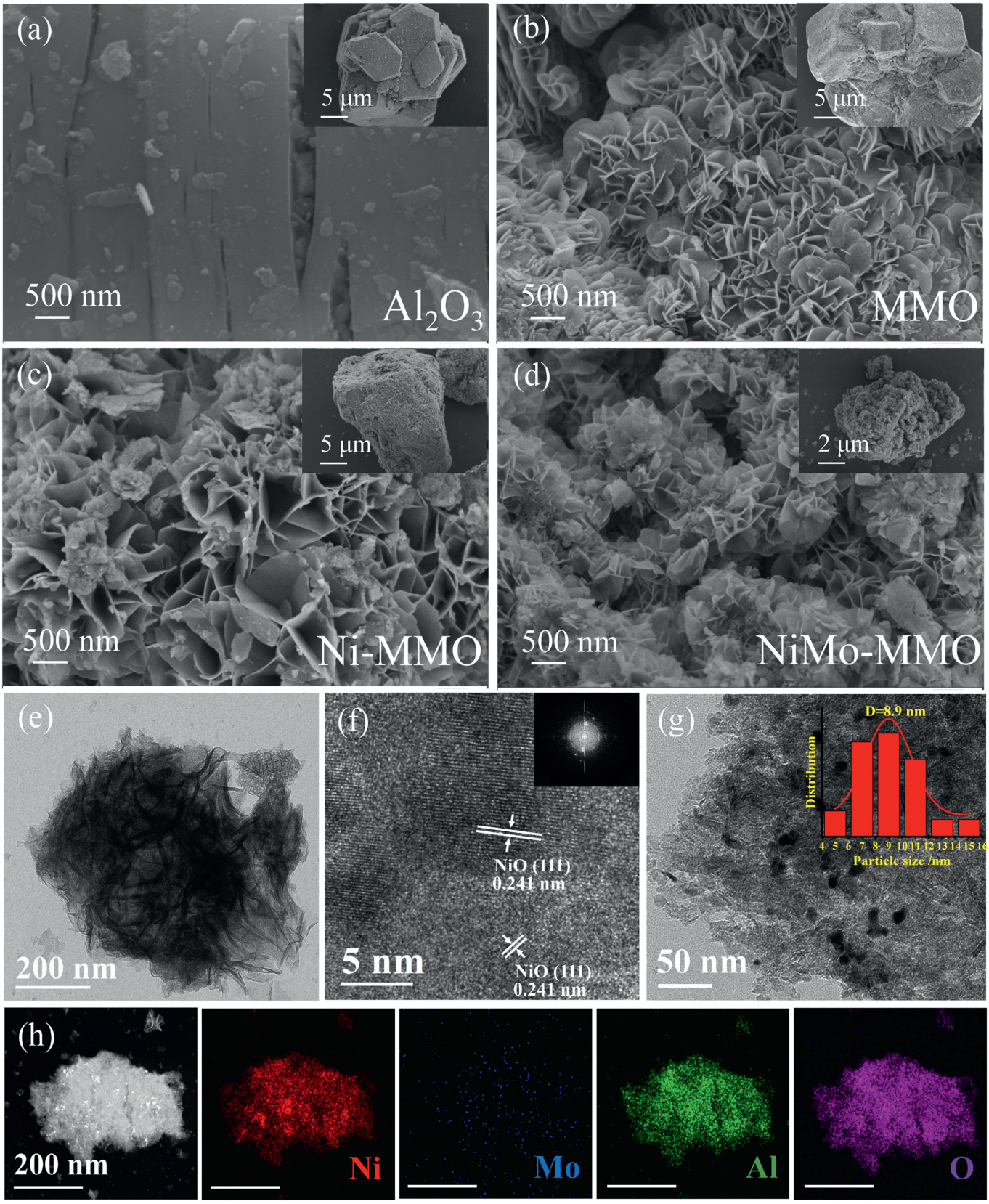

Fig. 2. SEM images (a–d) of pristine Al_2O_3 and Ni-based catalysts. TEM images (e–g) and EDX elemental mapping (h) images of NiMo-MMO catalyst.

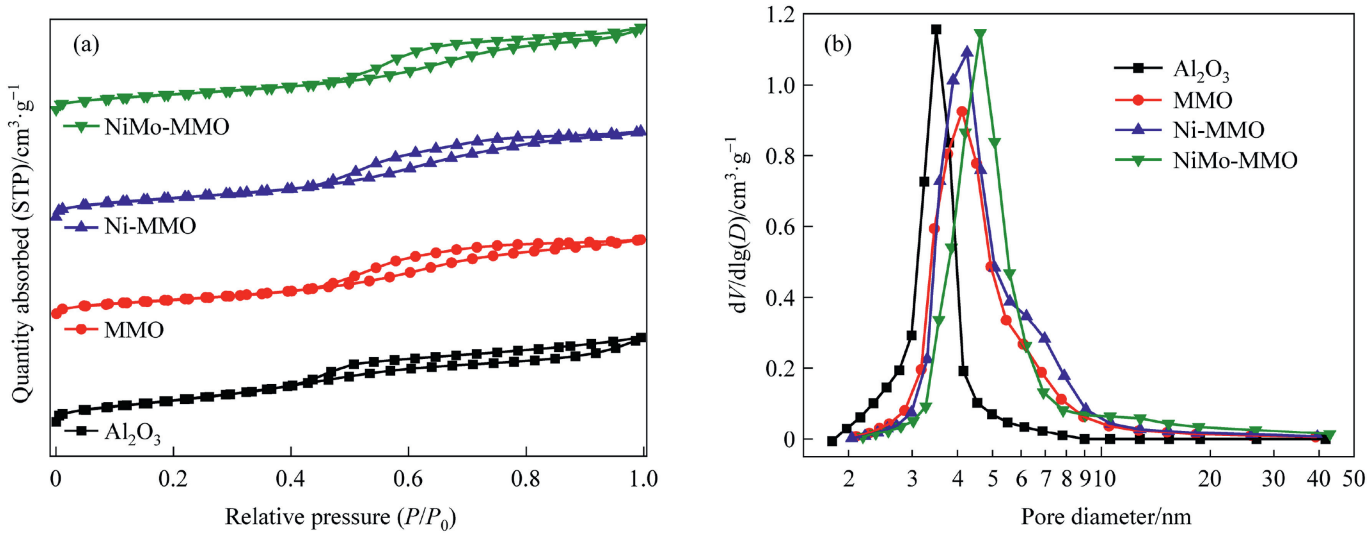

Fig. 3. N_2 adsorption-desorption isotherm (a) and BJH pore size distribution curves (b) of the various samples.

Table 2
The BET surface area (S_{BET}), pore volume and averaged pore diameter (APD)

Sample	S_{BET}/m^2·g^{-1}	Pore volume/cm^3·g^{-1}	APD/nm
Al_2O_3	150.30	0.24	6.44
MMO	135.28	0.21	6.34
Ni-MMO	166.51	0.25	5.91
NiMo-MMO	142.50	0.24	6.62

aggregation of active Ni species, and the larger ionic radius of Ni^{2+} on the sample surface occupies more space, which is in good agreement with the SEM and TEM results. The high BET surface area and pore volume was obtained for Ni-MMO, indicating the ammonium fluoride modification increases the specific surface area of the catalyst and optimized the pore structure. For the NiMo-MMO catalyst, which performs relatively high BET surface area, large pore volume, and the largest average pore size, which is favorable to the dispersion of the active species on the support [21].As it showed in the above SEM and TEM images, NiMo-MMO catalyst exhibits a high mesoporous random stacked nanosheet morphology, uniform nanoparticles size along with relative narrow pore size distribution, which could improve the dispersion exposure of the active species, and good for the mass transfer of PY during the hydrogenation process, thus promotes the deep hydrogenation of PY.

3.1.3. XRD analysis

Fig. 4 shows the XRD patterns of the prepared catalysts. Characteristic diffraction peaks occurred at 2θ of around 20.2°, 37.3°, 45.5° and 67.0° correspond to (1 1 1), (3 1 1), (4 0 0) and (4 4 0) planes of Al_2O_3 (PDF#No.10-0425) [22], respectively. For the Ni-based catalysts, three diffraction peaks at 37.2°, 43.3° and 62.9° assigned to NiO crystal planes of (1 1 1), (2 0 0) and (2 2 0) (PDF#No.47-1049), respectively. Meanwhile, the $NiAl_2O_4$ (PDF#No.10-0339) crystalline phase was found on the Ni-based catalysts, which would definitely benefit the improvement of the thermal stability and the protection of the active phase [23]. As shown in Fig. 4, the XRD patterns of the catalysts located around 37.2° is attributed to NiO (1 1 1) and $NiAl_2O_4$ (3 1 1), which are overlapped each other as a consequence of its highly dispersive nature. For the NiMo-MMO catalyst, it could be clearly seen that the peak of $NiAl_2O_4$ (1 1 1) is significantly enhanced. This suggests that the interaction between Ni species and the support is stronger with the addition of Mo [24]. However, there is no characteristic diffraction peaks of Mo species were observed in the XRD patterns of the NiMo-MMO catalyst. This may be caused by the low loading of Mo and the homogeneous dispersion [25].

3.1.4. XPS analysis

The chemical state and the surface composition of Ni-based catalysts were analyzed by XPS. The Ni 2p spectrum of MMO, Ni-MMO, and NiMo-MMO are shown in Fig. 5(a), (b) and (c), respectively. Peaks around 855.8 eV and 873.7 eV are corresponding to Ni^{2+} $2p_{3/2}$ and $2p_{1/2}$ peaks, respectively, while 862.16 and 880.14 eV are the characteristic satellite peaks of Ni^{2+} [26]. For the Ni-MMO catalyst, the Ni 2p spectrum shifted to lower energy range, indicating that the interaction between Ni species and the support was enhanced by loading Ni, thus the arrangement of Ni 2p connections within the support surface lattice has changed [27]. Doping Mo can increase the electron density of Ni on the sample surface and enhance its electronegativity, which affects the chemical environment of Ni, resulting in a left-shift of the Ni 2p spectrum of Ni—Mo bimetallic catalyst [28]. Additionally, the Ni^{2+} $2p_{3/2}$ peak slightly shift to high energy range in the XPS spectrum of Ni—Mo bimetallic catalyst, which might be attributed to the existence of direct or indirect electronic interaction between Ni and Mo [29]. The spectra of Mo 3d for NiMo-MMO catalyst was shown in Fig. 5(d), which can be fitted into 231.1eV (Mo^{5+} $3d_{3/2}$), 231.9eV (Mo^{4+} $3d_{5/2}$), 233.5eV (Mo^{6+} $3d_{5/2}$), 234.5 eV (Mo^{5+} $3d_{5/2}$) and 236.7eV (Mo^{6+} $3d_{3/2}$), respectively. Among them, the higher valence Mo^{4+}, Mo^{5+} and Mo^{6+} are attributed to the formation of molybdenum oxides by surface oxidation of Mo species [30]. The peaks at 234.7 and 235.2 eV of Mo 3d spectrum are probably formed by the partial fusion of the Mo oxide phase with the support [31]. The surface chemistry of the samples obtained from XPS analysis shown in Table 3. It can be observed that there is a higher Ni $2p_{3/2}$/Ni $2p_{1/2}$ ratio on the surface of the NiMo-MMO catalyst. The presence of active Ni species is extremely important for hydrogenation reaction because the Lewis acid active sites of the catalysts was pointed out as the key function of the catalyst [4]. The increase of Ni^{2+} $2p_{3/2}$ content favors the enhancement of electronegativity in active sites, making them more susceptible to adsorb aromatic hydrocarbons substrates [28]. The Mo species of NiMo-MMO are mainly assigned to the oxidized states Mo^{4+}, Mo^{5+} and Mo^{6+}, which play a role on the Ni-enrichment of the catalyst surfaces [32]. They are easily

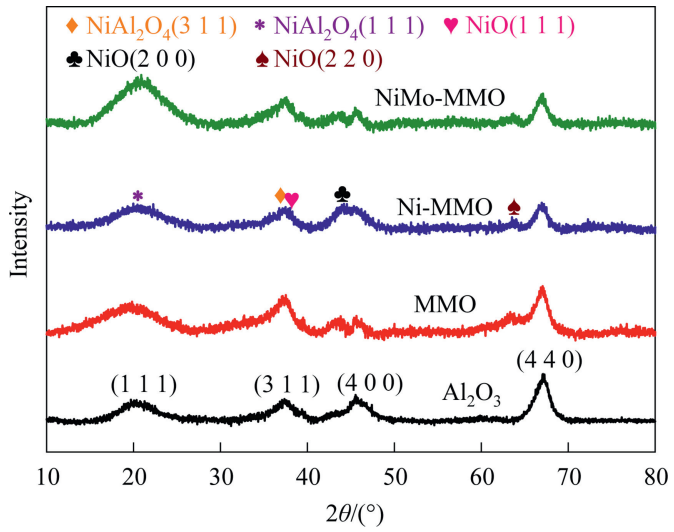

Fig. 4. XRD patterns of Ni-based catalysts.

transformed into relatively stable Mo^{4+} during hydrogenation process, and the higher Mo^{4+} content of NiMo-MMO could be attributed to the weaker molybdenum-support interaction, which favors the hydrogen molecules are dissociated by the metallic function to more active hydrogen atoms [33], thus facilitated the hydrogenation activity of the NiMo-MMO catalyst.

3.1.5. NH_3-TPD analysis

Fig. 6 shows NH_3-TPD profiles of the Ni-based catalysts. The results show that three ammonia characteristic desorption peaks appear for all sample, which are the weak, intermediate and strong acid sites concentrates in the 100–300 °C, 300–600 °C and above 600 °C, respectively. The type and the amount of acid sites are listed in Table 4. Compared to Al_2O_3, the addition of Ni generates more amount of weak acid sites over the catalysts. Moreover, with the increase of Ni content, strong acid sites are formed over both MMO and NiMo-MMO catalysts, while the quantity of weak and intermediate acid sites gradually decreases. The reason is that the Ni species were involved in a strong interaction with the support, and the dispersion and exposure of Ni species increased [34]. This led to

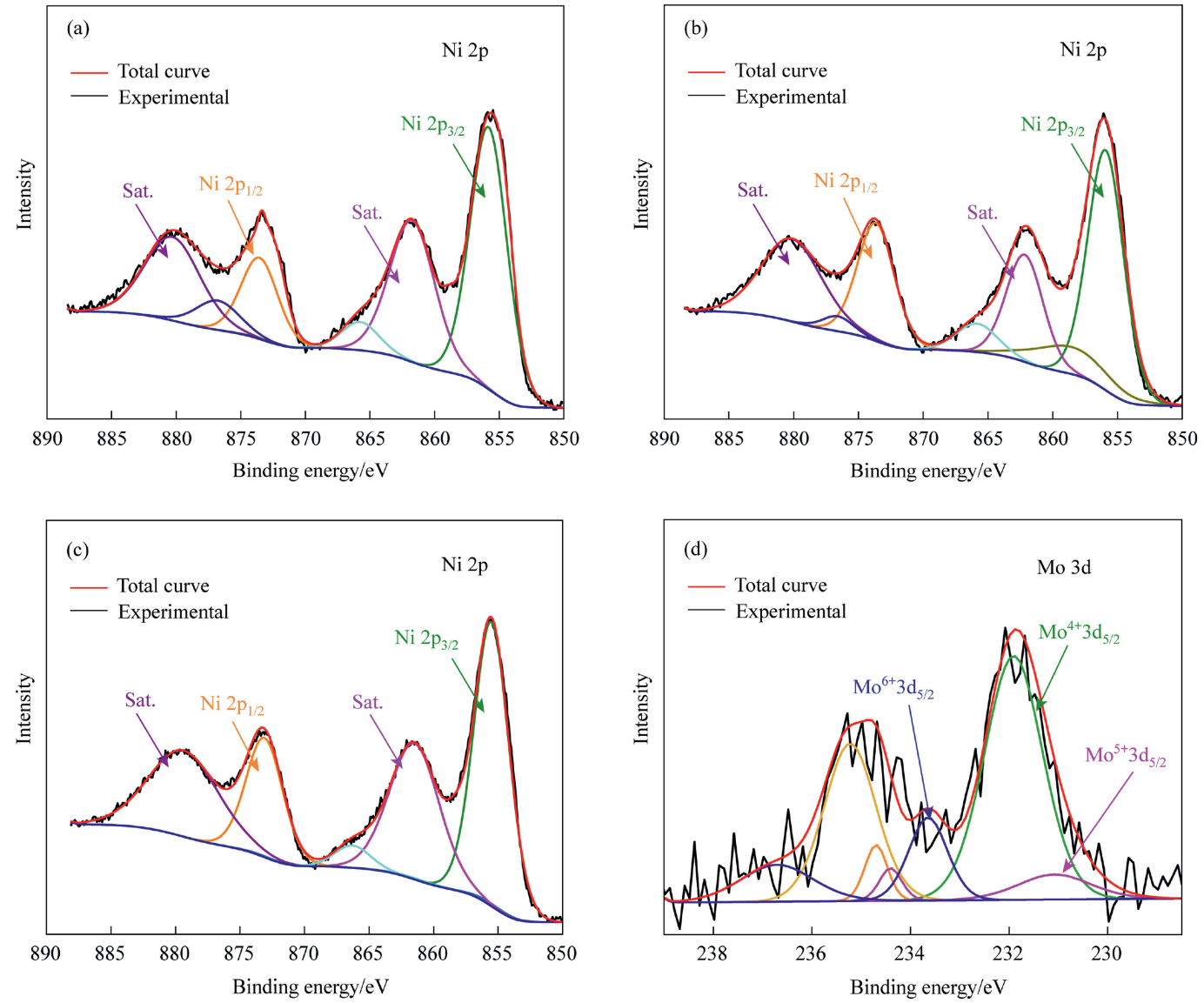

Fig. 5. Ni 2p XPS of various samples: (a) MMO, (b) Ni-MMO, (c) NiMo-MMO and (d) Mo 3d XPS of NiMo-MMO.

the part of weak and intermediate acid sites of the catalyst was covered by the active species, forming the new strong acid sites [35]. Moreover, compared with the Ni-MMO catalyst, the preferable interaction between Ni and Mo of NiMo-MMO catalyst as discussed in XPS might be responsible for the more intermediate and strong acid sites. It is clear that the interaction between Ni and Mo significantly influence the strength and/or number of acid sites on the catalyst surface. As a result, the NiMo-MMO catalyst exhibits good catalytic hydrogenation properties.

Table 3
Surface compositions obtained from XPS analysis data

Sample	Ni $2p_{3/2}$/Ni $2p_{1/2}$	Mo^{4+}/Mo^{6+}	Mo^{5+}/Mo^{6+}	Mo^{4+}/Mo^{5+}
MMO	0.19	—	—	—
Ni-MMO	0.50	—	—	—
NiMo-MMO	0.62	2.00	0.57	3.50

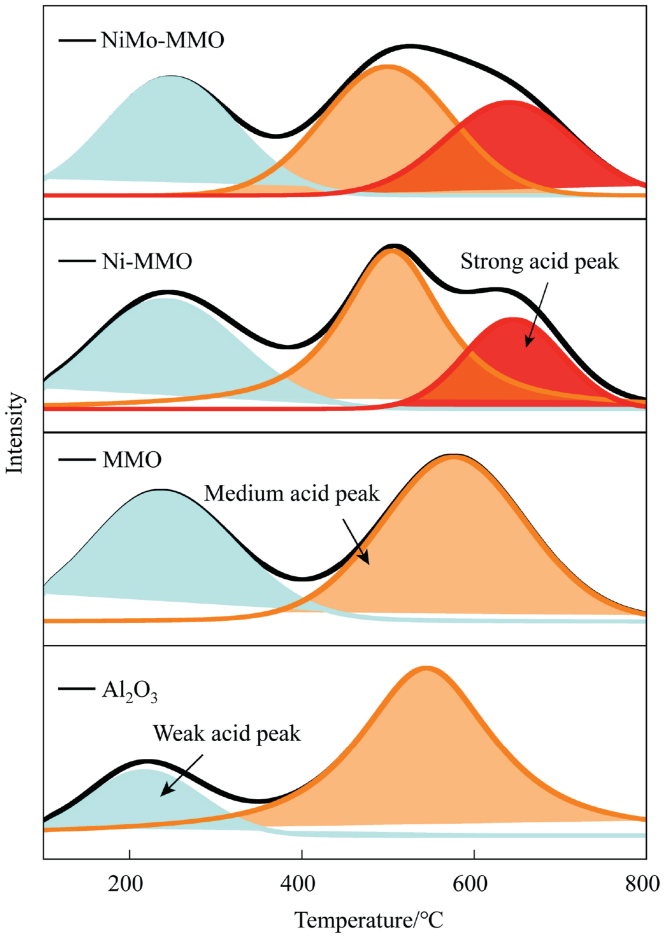

Fig. 6. NH_3-TPD profiles of pristine Al_2O_3 and Ni-based catalysts.

3.1.6. Pyridine-IR analysis

The type and the quantity of acid sites over the samples were investigated by Py-IR, and the results are shown in Fig. 7 and Table 5. The absorption bands at 1448 cm^{-1}, 1610 cm^{-1} and 1614 cm^{-1} are assigned to the bonding of pyridine molecules to Lewis (L) acid sites, whereas the absorption band at 1490 cm^{-1} is generated by the co-adsorption of pyridine at the Lewis and Brønsted (B) acid sites [36]. There is no characteristic peak at 1540 cm^{-1}, indicating that the acid properties of the prepared catalysts dominant by the L-acid sites. The data in Table 5 shows that the amounts of L-acid sites increased with the Ni loading. It also can be observed that the addition of Mo further facilitates the formation of L-acid sites. Meanwhile, combined with the results of NH_3-TPD analysis, it can be seen that the total amount of Lewis medium-strong acidity sites on the NiMo-MMO catalyst is higher than on other catalysts. The tetracyclic aromatic hydrocarbon pyrene has large π bond, which can be regarded as a Lewis base in an electron-rich state. Therefore, the sufficient L-acid sites promoted

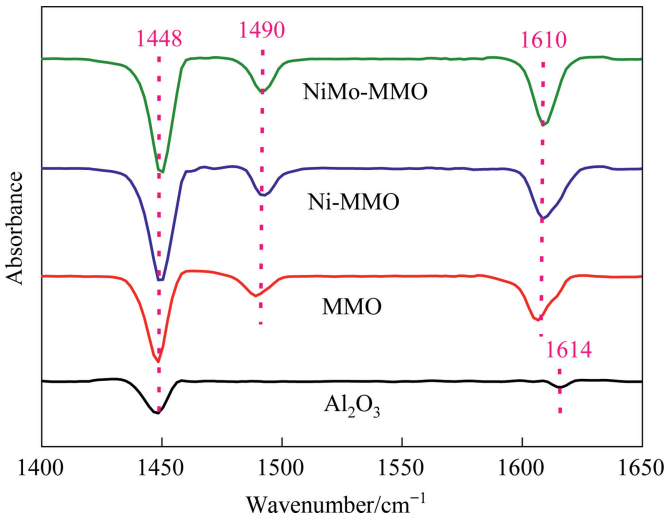

Fig. 7. Py-IR spectra of Ni-based catalysts.

Table 5
Py-IR quantitative analysis of Ni-based catalysts

Sample	Acidity amount/μmol·g^{-1}		
	Lewis acid sites	Brønsted acid sites	L + B
Al_2O_3	0.085	—	0.085
MMO	0.163	—	0.163
Ni-MMO	0.251	—	0.251
NiMo-MMO	0.293	—	0.293

Table 4
Acidity site amounts of Ni-based catalysts

Sample	Acidity amount/μmol·g^{-1}			
	Weak acid sites	Medium acid sites	Strong acid sites	Total acid sites
Al_2O_3	179.11	482.59	–	661.70
MMO	243.02	311.87	–	545.89
Ni-MMO	197.09	178.80	113.84	489.73
NiMo-MMO	188.67	198.18	123.60	510.45

the adsorption of pyrene, while the Lewis medium-strong acidity sites contributed to the production of H species, thereby large quantity Lewis medium-strong acidity sites enhancing the catalytic hydrogenation of PY [37], which is in close accordance with the catalytic activity results in Fig. 8.

3.2. Catalytic hydrogenation of pyrene

Fig. 8 and Table 6 shows the hydrogenation conversion and selectivity of PY over Ni-based catalysts. For pristine Al_2O_3, the PY Conv. is 4.73%, with a small amount of hydrogenation products of DiHP and TeHP. For MMO catalyst, the PY conversion was increased to 31.93%, and there is an increase in TeHP, which may be due to the further hydrogenation of DiHP to TeHP. Meanwhile, the selectivity of DiHP and HeHP ranged from 93.30% to 6.70%–62.87% and 30.86%, respectively. The Ni-MMO catalyst exhibited an increase in both conversion and selectivity as the Ni loading increased. The results of H_2-TPR (Fig. S4 and Table S2) show that the loading of the Ni significantly alters the reduction properties of Ni species in Ni-based catalysts. The active Ni species is mainly due to the hydrogen spill-over on the free NiO species and $NiAl_2O_4$ spinel phase of the catalysts at reaction temperature, thus favored the dissociative adsorption of active Ni species to hydrogen molecules on catalysts. As attested in Table 6, the conversion of PY attained 69.40%, which is 37.47% higher than the MMO catalyst, and the selectivity of 6.25% for DeHP was detected in the hydrogenation product of the DHP in Ni-MMO catalyst, indicating that the deep hydrogenation performance of PY improved. The rise in activity of the Ni-MMO catalyst may be attributed to its higher surface area, greater amounts of active species, and abundant L-acid sites. Meanwhile, the selectivity of TeHP (13.45%) and HeHP (43.78%) increased gradually with the decrease of that of DiHP (35.77%). This is consistent with Chen *et al.*'s report [38] that catalytic hydrogenation over transition metals is usually dominated by the Horiuti-Polanyi mechanism, which involves hydrogen molecule dissociation followed by the sequential addition of atomic hydrogen to the substrate. Among all the catalysts employed, the NiMo-MMO catalyst exhibits the excellent catalytic activity, with the highest PY conversion of 95.18%, and the highest DHP selectivity of 90.12%. Notably, the selectivity towards HeHP (48.61%) and DeHP (38.07%) increased significantly with the disappearance of DiHP, and HHP emerged with a selectivity rate of 3.44%. Regarding hydrogenation catalyzed by Ni-based catalysts, the key to achieving excellent catalytic activity is to have more catalytically active sites. These sites promote hydrogen dissociation and activate more reactants, resulting in higher conversion rates and product selectivity. For NiMo-MMO catalyst, it contains both Ni–Mo bimetallic and mesoporous nanosheet structure MMO, the former creates the active center for the transfer of H species production, while the latter provides space for good dispersion of active sites and the mass transfer adsorption of PY. Therefore, NiMo-MMO provides excellent deep hydrogenation activity, and the results have shown that the addition of 'Mo' further improves the overall catalytic activity. Furthermore, the stability of the NiMo-MMO catalyst was assessed by recycling it five times under identical conditions. The results are presented in Fig. 9 and Table 7. With an increase in the number of catalyst cycles, the PY conversion remains above 50%. The DHP selectivity over the NiMo-MMO catalyst was higher than that of other catalysts in each cycle and stabilized at around 50.75% after five cycles of reactions. In addition, the stability of the NiMo-MMO catalyst decreases significantly in conversion during the second run. From the post-reaction of TEM (Fig. S2) characterization results, it is noted that no structural transformation or aggregation of Ni nanoparticles was observed in the NiMo-MMO spent catalyst. The amount of coke deposition was evaluated for different number of cycling runs were analyzed by TGA, as shown in Fig. S3. The results show that more conversion favors the formation of more coke due to the deposition of hydrogenation products of pyrene,

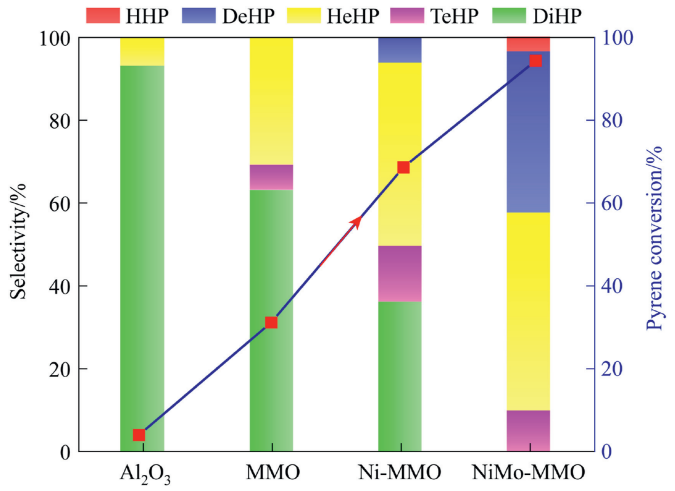

Fig. 8. Catalytic results for hydrogenation of pyrene over Ni-based catalysts.

Table 6
Pyrene hydrogenation performance over Ni-based catalysts

Sample	Conversion/%	Selectivity/%					
		DiHP	TeHP	HeHP	DeHP	HHP	DHP
Al_2O_3	4.73	93.30	—	6.70	—	—	6.70
MMO	31.93	62.87	6.28	30.86	—	—	30.86
Ni-MMO	69.40	35.77	13.45	43.78	6.25	—	50.03
NiMo-MMO	95.18	—	9.89	48.61	38.07	3.44	90.12

Table 7
Cycle-to-cycle reactions of hydrogenation of PY catalyzed by NiMo-MMO catalyst

Cycle index	NiMo-MMO catalyst[①]							
	Mass/g	Conversion/%	Selectivity/%					
			DiHP	TeHP	HeHP	DeHP	HHP	DHP
1	0.250	95.18	—	9.89	48.61	38.07	3.44	90.12
2	0.235	67.08	28.98	9.71	48.42	11.48	0.41	60.31
3	0.220	66.93	35.00	12.06	46.20	6.75	—	52.95
4	0.217	54.81	42.09	10.05	44.35	3.51	—	47.86
5	0.202	50.04	40.38	8.87	46.03	4.72	—	50.75

Reaction conditions: 1.0 g PY, 0.25 g catalyst, 34.0 g cyclohexane, 340 °C, 5.0 MPa H_2, 16 pm, 2 h.
① The catalyst was collected and dried at 80 °C for 2 h before reaction.

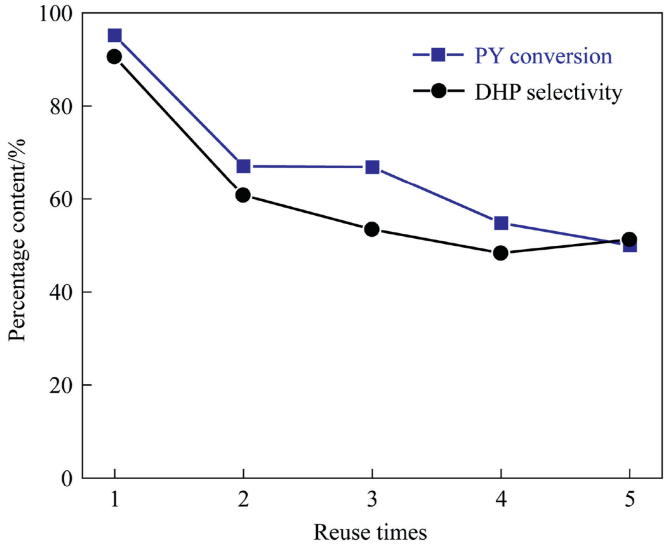

Fig. 9. The reusability evaluation of the NiMo -MMO catalyst.

thus the conversion markedly decreased in the second run. These results demonstrate the satisfactory stability and reusability of the NiMo-MMO catalyst in effectively improving DHP conversion.

4. Conclusions

In this work, three types of Ni-based catalysts with random stacked nanosheet structures were used for the deep catalytic hydrogenation of pyrene. The resulting NiMo-MMO catalyst exhibited an excellent catalytic activity with the PY Conv. (*ca*.95%) of which the selectivity to DHP is *ca*.90%. It was contributed to highly dispersed active species and large quantity Lewis medium-strong acidity sites, which is closely related to the synergistic effect between Ni and Mo. It is shown that the supported Ni and Mo metal modification increases the pore size of MMO and promotes the formation of more active sites, which act synergistically with the acid sites on the surface. High mesoporous random stacked nanosheet morphology of the catalyst not only facilitated the dispersion exposure of the active species, but also improved the mass transfer during the reaction process. The large quantity Lewis medium-strong acidity sites favored the activation of substrate molecules and the production of H species. Additionally, the synergistic effect enhances the interaction between the active species and support, and also favorable to increase the amount of the medium-strength acid. The low cost, simple preparation route and excellent deep hydrogenation catalytic activity make the NiMo-MMO catalyst have an important reference value in PAHs catalytic hydrogenation.

CRediT Authorship Contribution Statement

Yongliang Jia: Writing – original draft, Methodology, Conceptualization. Boyang Bai: Visualization, Methodology, Formal analysis. Jing Wang: Investigation. Yueyi Wang: Investigation. Zheng Wang: Investigation. Xiaoxun Ma: Supervision, Software, Project administration.

Declaration of Interest Statement

We declare that we have no financial and personal relationships with other people or organizations that can inappropriately influence our work, there is no professional or other personal interest of any nature or kind in any product, service and/or company that could be construed as influencing the position presented in, or the review of, the manuscript entitled. We declare that we have no conflicts of interest to this work.

Acknowledgements

This work was supported by the National Natural Science Foundation of China (21536009), Science and Technology Plan Projects of Shaanxi Province (2017ZDCXL-GY-10-03), and National Natural Science Foundation of China (22008198) and the Special Scientific Research Plan Project of Education Ministry of Shaanxi Province, China (19JK0854).

Supplementary Material

Supplementary data to this article can be found online at https://doi.org/10.1016/j.cjche.2024.09.010.

References

[1] BP Statistical Review of World Energy, 2023. https://www.bp.com/en/global/corporate/energy-economics/statistical-review-of-world-energy.html.
[2] X. He, G. Fan G, H. Wu, X. Zhang, T. Ma, Z. Shi, A. Zhou, Y. Zhang, Advances in research on hydrogenation saturation of polycyclic aromatic hydrocarbons in coal tar, *Coal Geol. Explor.* 52 (2024) 1–10.
[3] Z.H. Ma, X.Y. Wei, G.H. Liu, F.J. Liu, Z.M. Zong, Value-added utilization of high-temperature coal tar: a review, *Fuel* 292 (2021) 119954.
[4] M.L. Wang, X.Q. Qian, L.Q. Xie, H.H. Fang, L.M. Ye, X.P. Duan, Y.Z. Yuan, Synthesis of a Ni phyllosilicate with controlled morphology for deep hydrogenation of polycyclic aromatic hydrocarbons, *ACS Sustai. Chem. Eng.* 7 (2) (2019) 1989–1997.
[5] J.L. Gu, H. Li, Y.Q. Wu, S. Huang, S.Y. Wu, D.B. Chen, Preliminary investigations on the catalytic hydrogenation of polycyclic aromatic hydrocarbons *via* WGSR, *Mol. Catal.* 515 (2021) 111902.
[6] J.J. Liu, H.F. Zhang, N.Y. Lu, X.L. Yan, B.B. Fan, R.F. Li, Influence of acidity of mesoporous ZSM-5-supported Pt on naphthalene hydrogenation, *Ind. Eng. Chem. Res.* 59 (3) (2020) 1056–1064.
[7] Y. Chen, Z.M. Zhao, Z. Li, J.Y. Jing, W.Y. Li, Enhanced phenanthrene hydrogenation saturation performance of Ni-Co/NiAlO$_x$ catalysts and its catalytic mechanism, *Fuel Process. Technol.* 250 (2023) 107902.
[8] M.H. Stockett, L. Avaldi, P. Bolognesi, J.N. Bull, L. Carlini, E. Carrascosa, J. Chiarinelli, R. Richter, H. Zettergren, Competitive dehydrogenation and backbone fragmentation of superhydrogenated PAHs: a laboratory study, *Astrophys. J.* 913 (1) (2021) 46.
[9] B.Y. Bai, L.Y. Qiang, Y.L. Jia, X.X. Ma, Effect of nickel-based catalysts with nanolamellar structure on catalytic hydrogenation of pyrene: Combining experiment and calculation, *Fuel* 365 (2024) 131133.
[10] A.F.S. Zanato, V.C. Silva, D.A. Lima, M.J. Jacinto, Bimetallic magnetic PtPd-nanoparticles as efficient catalyst for PAH removal from liquid media, *Appl. Nanosci.* 7 (8) (2017) 781–791.
[11] G.Y. Zhang, Y.H. Wang, S.X. Dou, Y.Y. Dong, L.G. Ma, Q.Q. Zhu, X.J. Kong, MoO$_x$ regulating Ni-based catalyst anchored on N-doped carbon microspheres for catalytic hydrogenation of nitroarenes, *Sep. Purif. Technol.* 337 (2024) 126265.
[12] M. Xu, M. Wei, Layered double hydroxide-based catalysts: recent advances in preparation, structure, and applications, *Adv. Funct. Mater.* 28 (47) (2018) 1802943.
[13] R.M. Claydon, L.A. Roman-Ramirez, J. Wood, Comparative study on the hydrogenation of naphthalene over both Al_2O_3-supported Pd and NiMo catalysts against a novel LDH-derived Ni-MMO-supported Mo catalyst, *ACS Omega* 6 (30) (2021) 20053–20067.
[14] X.Y. Meng, Y.S. Yang, L.F. Chen, M. Xu, X. Zhang, M. Wei, A control over hydrogenation selectivity of furfural *via* tuning exposed facet of Ni catalysts, *ACS Catal.* 9 (5) (2019) 4226–4235.
[15] H.L. Zhang, J. Dong, X.L. Qiao, J.R. Qin, H.F. Sun, A.Q. Wang, L.B. Niu, G.Y. Bai, *In-situ* generated highly dispersed nickel nanoclusters confined in MgAl mixed metal oxide platelets for benzoic acid hydrogenation, *J. Catal.* 372 (2019) 258–265.
[16] Y. Tan, X.Y. Liu, L. Li, L.L. Kang, A.Q. Wang, T. Zhang, Effects of divalent metal ions of hydrotalcites on catalytic behavior of supported gold nanocatalysts for chemoselective hydrogenation of 3-nitrostyrene, *J. Catal.* 364 (2018) 174–182.
[17] R. Claydon, J. Wood, A mechanistic study of layered-double hydroxide (LDH)-derived nickel-enriched mixed oxide (Ni-MMO) in ultradispersed catalytic pyrolysis of heavy oil and related petroleum coke formation, *Energy Fuels* 33 (11) (2019) 10820–10832.
[18] S. Intachai, M. Na Nakorn, A. Kaewnok, P. Pankam, P. Sumanatrakul, N. Khaorapapong, Versatile inorganic adsorbent for efficient and practical

removal of hexavalent chromium in water, *Mater. Chem. Phys.* 288 (2022) 126388.
[19] Y.J. Li, T.T. Qi, Y.N. Dong, W.H. Hou, G.W. Chu, L.L. Zhang, B.C. Sun, Synthesized Ni/MMO catalysts *via* ultrathin Ni-Al-LDH in a rotating packed bed for hydrogenation of maleic anhydride, *Fuel* 326 (2022) 125035.
[20] W.P. Han, M.X. Tang, J.L. Li, X.K. Li, J.W. Wang, L.G. Zhou, Y. Yang, Y.Q. Wang, H. Ge, Selective hydrogenolysis of 5-hydroxymethylfurfural to 2, 5-dimethylfuran catalyzed by ordered mesoporous alumina supported nickel-molybdenum sulfide catalysts, *Appl. Catal. B Environ.* 268 (2020) 118748.
[21] N. Wang, K. Shen, L.H. Huang, X.P. Yu, W.Z. Qian, W. Chu, Facile route for synthesizing ordered mesoporous Ni–Ce–Al oxide materials and their catalytic performance for methane dry reforming to hydrogen and syngas, *ACS Catal.* 3 (7) (2013) 1638–1651.
[22] X.L. Wang, Z. Zhao, Z.T. Chen, J.M. Li, A.J. Duan, C.M. Xu, D.W. Gao, Z.K. Cao, P. Zheng, J.Y. Fan, Effect of synthesis temperature on structure-activity-relationship over NiMo/γ-Al_2O_3 catalysts for the hydrodesulfurization of DBT and 4, 6-DMDBT, *Fuel Process. Technol.* 161 (2017) 52–61.
[23] A.J. Pamphile-Adrian, F.B. Passos, P.P. Florez-Rodriguez, Systematic study on the properties of nickel aluminate ($NiAl_2O_4$) as a catalytic precursor for aqueous phase hydrogenolysis of glycerol, *Catal. Today* 394 (2022) 499–509.
[24] Z.G. Qiu, Q. Li, L. Shi, Z.Q. Li, L. Ding, L.F. Zhao, Effect of Ni loading and impregnation method on the hydrodenitrogenation of coal tar over Ni-Mo/γ-Al_2O_3, *Energy Sources Part A Recovery Util. Environ. Eff. (2020) 1–13.*
[25] N. Abdel Karim Aramouni, J. Zeaiter, W. Kwapinski, J.J. Leahy, M.N. Ahmad, Molybdenum and nickel-molybdenum nitride catalysts supported on MgO-Al_2O_3 for the dry reforming of methane, *J. CO_2 Util.* 44 (2021) 101411.
[26] S. Song, S.K. Yao, J.H. Cao, L. Di, G.J. Wu, N.J. Guan, L.D. Li, Heterostructured Ni/NiO composite as a robust catalyst for the hydrogenation of levulinic acid to γ-valerolactone, *Appl. Catal. B Environ.* 217 (2017) 115–124.
[27] Z.M. Shi, C.S. Wan, M. Huang, J.H. Pan, R.Z. Luo, D.L. Li, L.L. Jiang, Characterization and catalytic behavior of hydrotalcite-derived Ni–Al catalysts for methane decomposition, *Int. J. Hydrog. Energy* 45 (35) (2020) 17299–17310.
[28] W. Liu, Y.S. Yang, L.F. Chen, E.Z. Xu, J.M. Xu, S. Hong, X. Zhang, M. Wei, Atomically-ordered active sites in NiMo intermetallic compound toward low-pressure hydrodeoxygenation of furfural, *Appl. Catal. B Environ.* 282 (2021) 119569.
[29] L.H. Zhao, K.G. Fang, D. Jiang, D.B. Li, Y.H. Sun, Sol–gel derived Ni–Mo bimetallic carbide catalysts and their performance for CO hydrogenation, *Catal. Today* 158 (3–4) (2010) 490–495.
[30] L.L. Ji, J.Y. Wang, L.X. Guo, Z.F. Chen, *In situ* O_2-emission assisted synthesis of molybdenum carbide nanomaterials as an efficient electrocatalyst for hydrogen production in both acidic and alkaline media, *J. Mater. Chem. A* 5 (10) (2017) 5178–5186.
[31] D.S. Kim, K. Segawa, T. Soeya, I.E. Wachs, Surface structures of supported molybdenum oxide catalysts under ambient conditions, *J. Catal.* 136 (2) (1992) 539–553.
[32] P.M. Yeletsky, T.R. Reina, O.A. Bulavchenko, A.A. Saraev, E.Y. Gerasimov, O.O. Zaikina, J.M. Bermúdez, P. Arcelus-Arrillaga, V.A. Yakovlev, M. Millan, Phenanthrene catalytic cracking in supercritical water: effect of the reaction medium on NiMo/SiO_2 catalysts, *Catal. Today* 329 (2019) 197–205.
[33] R.G. Kukushkin, O.A. Bulavchenko, V.V. Kaichev, V.A. Yakovlev, Influence of Mo on catalytic activity of Ni-based catalysts in hydrodeoxygenation of esters, *Appl. Catal. B Environ.* 163 (2015) 531–538.
[34] P. Zhang, X.J. Yang, X.L. Hou, J.L. Mi, Z.Z. Yuan, J. Huang, C. Stampfl, Active sites and mechanism of the direct conversion of methane and carbon dioxide to acetic acid over the zinc-modified H-ZSM-5 zeolite, *Catal. Sci. Technol.* 9 (22) (2019) 6297–6307.
[35] Q. Zhao, W.H. Yang, J.J. Luo, C.H. Liang, Regulation of Ni/Al_2O_3 catalysts by metal deposition procedures for selective hydrogenation of adiponitrile, *New J. Chem.* 46 (4) (2022) 1498–1506.
[36] R.Y. Zhao, L.Y. Zeng, J. Liang, C.G. Liu, Interaction between Ni promoter and Al_2O_3 support and its effect on the performance of NiMo/γ-Al_2O_3 catalyst in hydrodesulphurization, *J. Fuel Chem. Technol.* 44 (5) (2016) 564–569.
[37] C.W. Dong, C.L. Yin, T.T. Wu, Z.Y. Wu, D. Liu, C.G. Liu, Study on the modification of unsupported hydrodesulfurization catalysts by the ZSM-5 zeolite nanoclusters, *Appl. Catal. Gen.* 582 (2019) 117113.
[38] Y.D. Chen, C.M. Li, J.Y. Zhou, S.T. Zhang, D.M. Rao, S. He, M. Wei, D.G. Evans, X. Duan, Metal phosphides derived from hydrotalcite precursors toward the selective hydrogenation of phenylacetylene, *ACS Catal.* 5 (10) (2015) 5756–5765.